HHS Public Access

Author manuscript

Phys Med Biol. Author manuscript; available in PMC 2019 December 19.

Published in final edited form as:

Phys Med Biol. ; 64(1): 015003. doi:10.1088/1361-6560/aaf453.

Monte Carlo study on optimal breast voxel resolution for dosimetry estimates in Digital Breast Tomosynthesis

Christian Fedon[1,*], **Carolina Rabin**[2,*], **Marco Caballo**[1], **Oliver Diaz**[3], **Eloy García**[4], **Alejandro Rodríguez-Ruiz**[1], **Gabriel A. González-Sprinberg**[2], and **Ioannis Sechopoulos**[1,5]

[1] Department of Radiology and Nuclear Medicine, Radboud University Medical Centre, Geert Grooteplein 10, 6525 GA, Nijmgen, The Netherlands [2] Instituto de Física, Facultad de Ciencias, Universidad de la República, Iguá 4225, Montevideo 11600, Uruguay [3] Computer vision and robotics institute, University of Girona, Campus Montilivi, 17071 Girona, Spain [4] Robotics group, University of León, MIC, 24071 León, Spain [5] Dutch Expert Centre for Screening (LRCB), Wijchenseweg 101, 6538 SW, Nijmegen, The Netherlands

Abstract

Digital Breast Tomosynthesis (DBT) is currently used as an adjunct technique to Digital Mammography (DM) for breast cancer imaging. Being a quasi-3D image, DBT is capable of providing depth information on the internal breast glandular tissue distribution, which may be enough to obtain an accurate patient-specific radiation dose estimate. However, for this, information regarding the location of the glandular tissue, especially in the vertical direction (i.e. x-ray source to detector), is needed. Therefore, a dedicated reconstruction algorithm designed to localize the amount of glandular tissue, rather than for optimal diagnostic value, could be desirable. Such a reconstruction algorithm, or, alternatively, a reconstructed DBT image classification algorithm, could benefit from the use of larger voxels, rather than the small sizes typically used for the diagnostic task. In addition, the Monte Carlo (MC) based dose estimates would be accelerated by the representation of the breast tissue with fewer and larger voxels. Therefore, in this study we investigate the optimal DBT reconstructed voxel size that allows accurate dose evaluations (i.e. within 5%) using a validated Geant4-based MC code. For this, sixty patient-based breast models, previously acquired using dedicated breast computed tomography (BCT) images, were deformed to reproduce the breast during compression under a given DBT scenario. Two re-binning approaches were applied to the compressed phantoms, leading to isotropic and anisotropic voxels of different volumes. MC DBT simulations were performed reproducing the acquisition geometry of a SIEMENS Mammomat Inspiration system. Results show that isotropic cubic voxels of 2.73 mm size provide a dose estimate accurate to within 5% for 51/60 patients, while a comparable accuracy is obtained with anisotropic voxels of dimension 5.46 × 5.46 × 2.73 mm^3. In addition, the MC simulation time is reduced by more than half in respect to the original voxel dimension of 0.273 × 0.273 × 0.273 mm^3 when either of the proposed re-binning approaches is used. No significant differences in the effect of binning on the dose

*These authors contributed equally to this work

DISCLOSURE OF CONFLICTS OF INTEREST

IS has a research agreement with Siemens Healthcare, Forchheim, Germany, unrelated to this work.

estimates are observed (Wilcoxon-Mann-Whitney test, p-value > 0.4) between the 0° the 23° (i.e. the widest angular range) exposure.

Keywords

Breast Dosimetry; Monte Carlo simulation; Digital Breast Tomosynthesis; Voxel Binning; Patient-specific dosimetry

I. INTRODUCTION

Digital Mammography (DM) is currently the mainstay for early detection of breast cancer in screening programs worldwide. Recently, Digital Breast Tomosynthesis (DBT) has been introduced to potentially complement or even replace DM in breast screening scenarios (Michell *et al* 2012, Skaane *et al* 2012, Ciatto *et al* 2013, Houssami and Skaane 2013, Rafferty *et al* 2013, Skaane *et al* 2013, Conant 2014, Friedewald *et al* 2014, Lång *et al* 2016). Consequently, in the US, DBT is currently employed as the imaging modality of choice for screening, while its introduction in European population screening programs may occur in the near future.

Currently, breast dosimetry is performed by modelling the breast as a homogeneous and uniform mixture of adipose and glandular tissue, surrounded by a layer of adipose (Dance 1990) or skin material (Wu *et al* 1991, Boone 1999). Although these models try to reproduce the average density of the whole breast, it has been demonstrated that these homogeneous breast models lead, on average, to an overestimation of 30%, and overestimates of 120% are possible, in the breast glandular dose (Sechopoulos *et al* 2012, Hernandez *et al* 2015). Moreover, the average breast density, usually considered as a homogenous mixture composition of 50% glandular tissue and 50% adipose tissue, is not representative of the real average breast density (Yaffe *et al* 2009). Although breast dosimetry calculations using the homogeneous tissue mixture approximation is useful for many applications, its limitations, especially for use in absolute terms, need to be taken into account (Dance and Sechopoulos 2016).

Knowledge on the spatial distribution of the glandular tissue of the breast through DBT imaging, especially in the vertical (i.e. x-ray source to detector) direction, would allow to estimate the specific average glandular dose to the imaged breast, by simulating the acquisition process by means of a Monte Carlo (MC) approach. These patient-specific dose estimates could be useful to improve the modeling of radiation risk, to lead to a better dose estimate, and to improve quality assurance achievable via dose registries similar to the American College of Radiology CT dose index registry.

In order to obtain such patient-specific breast dose estimate, localization of the glandular tissue is needed. Due to the limited angular range used for DBT acquisition (current maximum of ~46°), reconstructed DBT slices are considered quasi-3D images (Sechopoulos 2013a, 2013b). Typically, in a DBT system, the breast volume is reconstructed to pixel sizes of approximately 0.1×0.1 mm^2, with 1 mm separation between slices. Therefore, DBT images can, in principle, provide enough information on the actual breast tissue structure

and location (Pöhlmann *et al* 2017) to be able to obtain a patient-specific average glandular dose estimate. In light of this, a first step is to optimize the breast voxel size needed for the breast model used in the MC simulation. Obtaining a breast representation for dosimetry estimation with voxels larger than those used for image interpretation has two potential benefits. In the first place, the automated tissue classification, i.e. skin, adipose and glandular tissue, from DBT reconstruction slices, or the reconstruction directly to classified voxels, might be easier. This is due to the possibility of signal averaging, resulting in lower noise in each voxel, which might aid the classification/reconstruction process. Secondly, the MC dosimetry simulation would be accelerated since fewer number of voxels (i.e. path calculations) would be involved during the MC simulations.

Therefore, the aim of this work is to determine the trade-off between classified DBT voxel size and dose estimation accuracy using Monte Carlo simulations of DBT acquisitions with breast models based on patient dedicated breast CT images.

II. MATERIAL AND METHODS

To perform this study, a dataset composed of 3D images, acquired using a dedicated breast Computed Tomography system (BCT), were used. BCT images were used since they provide very good estimates of the 3D real distribution of the fibroglandular tissue within the breast, with isotropic spatial resolution higher than other 3D technologies (such as magnetic resonance). The images were automatically segmented and their mechanical compression simulated, by means of a finite element approach, to replicate DBT acquisition. A MC simulation was performed in order to estimate the glandular dose.

By varying the binning of the voxels defining the internal breast tissue structures, and repeating the MC simulation, the error in the glandular dose estimation, along with the simulation speed-up was analyzed. The process used to evaluate the optimal voxel size for breast dose estimation is shown in Figure 1. Further details of this methodology are provided below.

II.A Breast model

II.A.1 Image acquisition—Sixty BCT images were acquired from 60 patients as part of an ongoing ethics board-approved study. Informed consent to use these images for further research, after anonymization, was obtained from all patients. All BCT images were acquired by trained radiographers using a dedicated BCT clinical prototype (Koning Corp., West Henrietta, NY), currently installed at Radboud University Medical Centre (Nijmegen, The Netherlands). Details on the BCT prototype are described in Ning *et al* (2007), which can be summarized as follows.

The x-ray tube of the BCT system includes a tungsten target and aluminium filter, and operates at a fixed voltage of 49 kV, resulting in a first half value layer of 1.39 mm Al with a 0.3 mm nominal focal spot. The tube operates in a constant 8 ms pulse mode with a tube current automatically set for each patient after the acquisition of two scout images normal to each other. The system is equipped with a flat panel digital x-ray detector (4030CB, Varian Medical Systems, Palo Alto, CA), positioned at 923 mm from the x-ray source. A complete

BCT scan involves the acquisition of 300 projections over a full 360° revolution of the x-ray tube and detector around a vertical axis located at 650 mm from the x-ray source. The dose delivered during the acquisition varies for each patient breast as described by Sechopoulos *et al* (2010). All images were reconstructed using a Filtered Back Projection algorithm in a volume with isotropic 0.273 mm voxels.

II.A.2 Tissue classification—The voxels in the reconstructed BCT images were automatically classified into four categories: air, skin, adipose and glandular tissue. A detailed description of the algorithm is presented in Caballo *et al* (2018). Briefly, the algorithm combines region-based segmentation approaches with energy minimizing frameworks, segmenting each tissue independently slice-by-slice, in an unsupervised manner. First, the skin of the breast is detected and segmented using a constrained region-growing algorithm based on intensity thresholding and multiscale second order features. For adipose-glandular tissue discrimination, a region-based active contour model is adopted, which has been shown to be robust to image non-uniformities and local optima convergence. The whole algorithm was tested on two different image datasets (Caballo *et al* 2018) acquired with different breast CT devices, and resulted to be reasonably robust to image noise, cupping artefacts and incomplete scatter correction.

The total mass of the glandular and adipose tissue included in the BCT images was calculated from the segmented images for each patients by counting the number of voxels classified as glandular and adipose tissue, and multiplying them by the given voxel size and the corresponding tissue density (adipose, ρ_a: 0.93 g/cm^3 and glandular, ρ_g: 1.04 g/cm^3, as described by Hammerstein *et al* (1979)). The breast density (BD) is obtained as the ratio between the glandular tissue and the whole breast mass, as follows:

$$\mathrm{BD} = \frac{n_g \cdot V \cdot \rho_g}{\left(n_g \cdot V \cdot \rho_g + n_a \cdot V \cdot \rho_a\right)}, \quad (1)$$

where n_g *and* n_a are the number of voxels classified as glandular and adipose tissue respectively, and V is the voxel volume.

II.A.3 Mechanical compression simulation—Classified BCT images were converted into a finite element (FE) biomechanical model in order to simulate the breast compression performed during the mammographic procedure. The FE biomechanical model was generated using the package iso2mesh (v.1.8; Matlab v.13a). A large number of 4-node tetrahedral elements, between 100k and 500k, were used in order to minimise the numerical error during the FE analysis (Palomar *et al* 2008).

Nearly incompressible (Poisson ratio equal to 0.495), homogeneous and isotropic Neo-Hookean material models for each tissue were used to describe their mechanical behaviour. The Young's modulus for glandular, adipose and skin tissue were set to 4.46 kPa, 15.1 kPa, and 60 kPa, respectively (Wellman 1999). The mechanical compression was then simulated using the open-source package NiftySim (v.2.3.1; University College London) (Johnsen *et al*

2014). NiftySim uses a Total Explicity Dynamic Lagrangian approach to solve the mechanical FE problem (Miller *et al* 2007).

In the compression process, the breast support and compression paddle were implicitly defined by means of two frictionless infinite linear planes. During the simulation, the breast support was moved up 20 mm to make the lowest part of the model flat, while the compression paddle was moved down until the desired breast thickness was reached. Each breast was compressed to the thickness recorded in the corresponding DICOM header of the cranio-caudal mammographic view of that breast, which was acquired, for clinical purposes, during the same visit as the acquisition of the BCT image. In addition, the displacement of the nodes belonging to the chest wall side surface was restricted to the chest wall plane.

A slow compression (10 seconds) was performed, dividing each second in 10,000 steps in order to produce a realistic tissue displacement during the simulation. In this sense, the Damping coefficient was set to 0.69 (Hsu *et al* 2011) and gravity was applied over time using polynomial behaviour. In order to construct the compressed breast phantom, a uniform grid was placed around the compressed model (Lagae and Dutre 2008) using the original voxel size of 0.273 mm. For each voxel of the grid, the corresponding barycentre coordinates were used to localize the initial position within the uncompressed breast model (García *et al* 2018) and the corresponding voxel label was obtained from the segmented BCT volume using nearest neighbour interpolation. It was observed that the maximum absolute breast density difference between the uncompressed and compressed breast was 1% across all breasts.

The simulation was performed in a 64-bit Intel Core i7–3770 3.40 GHz workstation, equipped with 32 GB RAM and a NVIDIA GeForce GTX 770 (2 GB) graphics processing unit (GPU). The GPU capabilities of NiftySim were used in order to speed up the process. The time required to synthesize the compressed breast image was, on average, 10 minutes. In Figure 1, an example of the initial classified BCT image and the breast after the compression process is presented.

II.A.4 Voxel resampling process—Prior to the voxel resampling process, the skin voxels (labelled during the tissue classification process) were automatically removed from the compressed images. After resampling and prior to the MC simulations, two 1.45 mm-thick skin layers (Huang *et al* 2008) were added at the top and at the bottom of the compressed breast to include the shielding effects of the skin (Massera and Tomal 2018), ensuring that the skin layers covered completely the breast model extent in the axial plane (i.e *XY*). The skin replacement with a constant-thickness skin layer across breast models was done to avoid any bias due to the variability in skin thickness among different patients (Huang *et al* 2008).

The compressed breast models were downsampled in all three dimensions by different factors (*fx, fy, fz*) following a box pooling rule. A maximum pooling rule was chosen, since the pixel values in the segmented images (i.e. tissue labels) were integers from 0 to 2 (i.e. air, adipose and glandular tissues, respectively). The new pixel values in the downsampled models [i.e. $(x, y, z)_{\text{downsampled}}$] were estimated as the mode values of its neighbouring

pixels [i.e. $(x \pm fx/2, y \pm fy/2, z \pm fz/2)_{original}$]. During this process, the original breast density is known *a priori* and it was set as a constrain. After the first iteration of the maximum pooling rule, if the breast density was lower than originally, a second maximum pooling was performed. In this second round of maximum pooling, if the glandular tissue was the second type of tissue with most pixels in that area, then the associated voxel in the downsampled model was assigned to glandular tissue. The process was repeated until the original breast density is recovered. For this reason, several voxels labelled as adipose in the downsampled model, were later assigned as glandular.

Two downsampling approaches were investigated: (i) isotropic-voxel binning (i.e. the downsampled voxels are cubic); (ii) anisotropic-voxel binning (i.e. the downsampling process occurred only in the XY axial plane), while keeping the depth resolution (Z plane) fixed. In particular, the five scenarios investigated in the two approaches are presented in Table 1.

Figure 2 visually illustrates the re-binning process on the XY axial plane applied to one example case.

II.B Monte Carlo simulations

A previously experimentally validated (Fedon *et al* 2018a, 2018b) MC simulation code for breast dosimetry (Sechopoulos *et al* 2007, Sechopoulos *et al* 2012), based on the Geant4 toolkit (release 10.03, December 2016) (Agostinelli *et al* 2003), was modified to match the characteristics of the DM/DBT system (Mammomat Inspiration, Siemens Healthcare, Forchheim, Germany) used to acquire the same patients' clinical DBT images. Figures 3 depict a cross section of the geometry used in the simulations, which reproduces the DBT acquisition at 0° degree and at 23° degree (i.e. maximum angular aperture).

The isotropic x-ray point source was located 655.5 mm above the detector and collimated to the 240 mm × 300 mm detector, and did not include the heel effect. The compression paddle and the breast support table were defined as a 3 mm-thick layer of polyethylene terephthalate (PET) and a 1.7 mm-thick layer of carbon fiber, respectively. The detector air gap (which also included the breast support table) was set to 17 mm. The distance between the center of rotation and the detector was equal to 47 mm. The compressed breast volume was placed at the centre of the x-ray field with the chest wall edge at the central ray, as is common in DBT geometries. No backscatter effect from the patient's body was included in the simulation. In each simulation, the voxel size varied as listed in Table 1, with the material assigned to each voxel being adipose or glandular breast tissue, using the description given by Hammerstein *et al* (1979).

The x-ray spectra were modelled following the $TASMICS_{M\text{-}T}$ model (Hernandez and Boone 2014), and different spectra were used for each simulated compressed breast thickness. The x-ray spectra used were varied to match the target/filter combination and tube voltage setting used for each patient mammogram, as listed in Table 2.

For each breast model, ten parallel runs of 10^7 x-rays were simulated and the photons were followed until they were completely absorbed or left the simulation volume. This number of

histories was enough to obtain an uncertainty of less than 0.1% (estimated using the method proposed by Sempau *et al* (2001)) in the total energy deposited within the whole glandular volume for all breast models. The physics interaction processes (i.e. photoelectric effect, coherent and incoherent scattering) were implemented in the MC code (Fedon *et al* 2015) using the EPDL97 library (Cullen *et al* 1997) by using the Geant4 electromagnetic Physics List Option 4*. The default cut range for photons was used (1 mm, corresponding to an energy of 2.45 keV and 2.88 keV in adipose and glandular breast tissue, respectively).

Each energy deposition event by means of photoelectric or incoherent scattering that occurred in the breast voxel marked as glandular tissue was recorded. The mean glandular dose (D) was then computed following the equation:

$$D = \frac{\sum_{i=1}^{N} e_i}{\left(n_g \cdot \rho_g \cdot V\right)}, \quad (2)$$

where e_i is the energy deposited in the glandular breast tissue by the i-th energy-depositing interaction, n_g is the number of glandular voxels, ρ_g is the density of glandular tissue, and V is the voxel volume. Differences in the effect of binning on the dose estimate between the two exposures (i.e. 0° and 23°) were assessed using a Wilcoxon-Mann-Whitney test.

The time required for each simulation was recorded to investigate the simulation-time performance as the voxel size was modified.

III. RESULTS

Figure 4 presents a scatter plot of the percentage glandular fraction (evaluated after the segmentation process) as function of the compressed breast thickness for the 60 patients.

III.A Isotropic-Voxel Binning

The normalized dose estimates for the cubic voxel sizes for 0° and 23° are illustrated in Figures 5.

Note that a 5% mean under-estimation in the dose is observed for the largest voxels (i.e. 5.460 × 5.460 × 5.460 mm^3), with respect to the reference dose level (i.e. 0.273 × 0.273 × 0.273 mm^3). However, as the voxel size increased, the variability in dose accuracy also increased (Figures 5a, 5b). In particular, a maximum deviance of ~25% was observed for the 4.095 × 4.095 × 4.095 mm^3 (i.e. 15×15×15) voxel for both exposure. A linear relationship is found between the increment on the cubic voxel size and the average dose under-estimate. The isotropic voxel size of 2.73 mm seems to achieve a good trade-off between voxel volume and dose accuracy, with 51/60 dose values (i.e. 85%) being within 5% of the true (non-binned) value. No significant differences in the effect of binning on the dose estimates were observed between 0° and 23° (Wilcoxon-Mann-Whitney test, minimum p-value = 0.44, among the several re-binning cases).

*http://geant4.cern.ch/collaboration/working_groups/electromagnetic/physlist10.0.shtml

Figures 6 report the range (i.e. the difference between maximum and minimum normalized dose values) as a function of the isotropic re-binning case for different breast density (Figure 6a) and compressed breast thickness (Figure 6b). Higher range variations were observed in the breast with low glandularity and higher breast thickness.

III.B Anisotropic-Voxel Binning

Figures 7 shows the normalized dose values estimated for different XY axial voxel sizes (voxel size in the Z direction was fixed to 2.73 mm) for 0° and 23°, respectively. Up to a 2% mean difference is observed when anisotropic re-binning on the XY axial plane (i.e. 20×20×10) is used. A linear relationship ($R^2 > 0.82$) is found between the increment on the XY axial voxel size and the average dose under-estimate. Overall, 47 out of the 60 normalized dose values (i.e. 78%) are within 5% dose accuracy for the 20×20×10 re-binning scenario. No significant differences in the effect of binning on the dose estimates were observed between 0° and 23° (Wilcoxon-Mann-Whitney test, minimum p-value = 0.69, among the several re-binning cases).

Higher dose range variation was also observed for the low dense breast (Figure 8a) and for thicker compress breast (Figure 8b) in the anisotropic re-binning approach.

III.C Simulations Time

An important reduction in the computer simulation time was observed when increasing the voxel size (Figures 9). A reduction of about ~50% of the simulation time, on average, can be obtained if a re-binning approach is used, compared with the original voxel size. The maximum simulation wall clock time for the non-binned breast model was 30 minutes (i.e. 5 CPU-hours, on a 3.0 GHz Intel Xeon CPU E5–2690 v2 computer).

IV. DISCUSSION

Modeling the breast by means of anisotropic voxels with size $5.46 \times 5.46 \times 2.73$ mm^3 leads to an average error in the dose estimate of 2%. For this voxel dimension, 47 cases result in dose estimates within 5% of the dose estimates for the original voxel volume. Comparable accuracy with isotropic voxels can only be achieved by using a cubic voxel with 2.73 mm sides. This result is in line with the fact that the dose strongly depends on the glandular distribution along the vertical direction (i.e. Z axis) (Sechopoulos *et al* 2012). Moreover, two aspects should be noted: (i) the inter-quartile ranges for the anisotropic voxels are more symmetric (Figures 7) than the isotropic ones (Figure 5); (ii) the normalized dose range varies as a function of breast density and voxel size (Figures 6a and 8a). Specifically, the range increases as the voxel size increases, and it decreases as breast density increases. A smaller range variation was observed for the anisotropic approach. These two facts confirm the dose estimate sensitivity to the Z dimension of the voxel.

Increasing compressed breast thickness leads to a higher range variation since thicker breasts tends to have lower density (see Figure 4). Thus, it seems that different voxel sizes could be selected according to breast density. For example, for dense (i.e. density >30%) and small breasts (i.e. compressed breast thickness < 50 mm), higher voxel sizes could be used than for fatty and thicker breast. However, given the relatively low number of cases included in this

study per category, it is challenging to provide category-specific voxel sizes and their resulting variations in dose estimation. This more personalized approach to binned dose estimation could be a topic for further future research.

Furthermore, it should be noted that the larger the voxel volume, the lower the MC simulation time, reaching half of the initial time (Figures 9). Specifically, the maximum simulation time of this work (ten parallel runs of 10^7 photons) was 5 CPU-hours for the smallest voxels, i.e. 0.273 mm cubic voxel size, which could be reduced to 2.5 CPU-hours, on average, via the binning process. It should be noted that these simulation times were used to achieve a precision of 0.1%, while for routine use it is common practice to perform MC estimates of glandular dose to 1% precision. Therefore, even for a precision of ~0.5%, with a current multi-core workstation and parallel MC code, the estimation of the total patient-specific glandular dose could be performed in under one minute.

When images are rebinned both in isotropic or anisotropic voxel, no significant difference in the effect of binning on the dose estimates was observed between the 0° and 23° exposure. Thus, no influence on the voxel size was found due to the angular variation in DBT. As expected, the actual dose estimates for the 0° exposure was always higher than 23° exposure (in agreement with the previous work of Sechopoulos *et al* 2007) confirming the need of a specific parameter that takes into account the DBT angle for Mean Glandular Dose estimate.

A potential limitation of this work is the relative low number of cases studied (60 women). Although this number of cases seems appropriate to recommend an upper limit in the binning factor, resulting in an upper limit in the underestimation of the patient-specific dose, this recommendation might not be optimal. Analysis like the one performed here for a considerable number of breasts could result in better estimates of the effect of binning specifically for varying types of breasts (e.g. thin, medium, or thick breasts; dense vs. non-dense breasts), and this could lead to varied binning factor recommendations for each of these breast types. However, the number of cases included in this study does provide enough insight as to result in an overall binning factor to be used for all breasts, perhaps a more conservative one than the one that could be used for some breasts.

In addition, this work has reproduced the geometry characteristics of only one system, although with several x-ray spectra, corresponding to the appropriate compressed breast thickness. The implementations of other system geometries and energy spectra could enhance the robustness of our results. However, given the factors that affect breast dosimetry, the use of different spectra, as was included here, is expected to be more important than the relatively minor geometrical differences among systems from different vendors.

V. CONCLUSIONS

Patient-specific dose estimates from DBT acquisitions can be obtained with high accuracy (i.e. less than a 5% error) using either cubic isotropic voxels of 2.730 mm in size or anisotropic voxels with dimension $5.460 \times 5.460 \times 2.730$ mm^3. These larger voxels can potentially allow for an easier classification or reconstruction due to their lower image noise.

Moreover, the information about the in-depth glandular tissue distribution, could be used to develop new models for breast dose estimate, as proposed by the Task Group/Work Group No. 282 formed by the American Association of Physicists in Medicine (AAPM) and the European Federation Of Organization for Medical Physics (EFOMP).

In addition, such binning processes result in a reduction of the MC simulation time by half. Finally, if both DBT and DM images are acquired during the same compression, the tissue location information obtained from the DBT image could be used to estimate the patient-specific average glandular dose from the DM acquisition.

ACKNOWLEDGMENT

This work has been supported by the Susan G. Komen Foundation for the Cure (IIR13262248) and in part by the National Cancer Institute (R01CA163746, R01CA181171). Authors would like to thank the Comisión Académica de Posgrado (CAP) and Comisión Sectorial de Investigación Científica (CSIC) under project C681. The content is solely the responsibility of the authors and does not necessarily represent the official views of the funding agencies.

REFERENCES

Agostinelli S and et al. 2003 Geant4 – A simulation toolkit Nucl. Instrum. Methods A 506 250–303

Boone JM 1999 Glandular breast dose for monoenergetic ad high energy x-ray beams: Monte Carlo assessment Radiology 213 23–37 [PubMed: 10540637]

Caballo M, Boone JM, Mann R and Sechopoulos I 2018 An unsupervised automatic segmentation algorithm for breast tissue classification of dedicated breast computed tomography images Med. Phys. 45(6) 2542–2559 [PubMed: 29676025]

Ciatto et al. 2013 Integration of 3D digital mammography with tomosynthesis for population breast-cancer screening (STORM): a prospective comparison study The Lancet Oncology 14(7) 583–589 [PubMed: 23623721]

Conant EF 2014 Clinical Implementation of Digital Breast Tomosynthesis Radiol. Clin North Am. 52(3) 499–518 [PubMed: 24792652]

Cullen D, Hubbell JH and Kissel L 1997 EPDL97: the Evaluated Photon Data Library, '97 version UCRL 6(5) 50400

Dance DR 1990 Monte Carlo calculation of conversion factors for the estimation of mean glandular breast dose Phys. Med. Biol 35 1211–1219 [PubMed: 2236205]

Dance DR and Sechopoulos I 2016 Dosimetry in x-ray-based breast imaging Phys. Med. Biol 61 R271–R304 [PubMed: 27617767]

Fedon C, Longo F, Mettivier G and Longo R 2015 GEANT4 for breast dosimetry: parameters optimization study Phys. Med. Biol 60 N311–N323 [PubMed: 26267405]

Fedon C, Caballo M, Longo R, Trianni A and Sechopoulos I 2018a Internal breast dosimetry in mammography: Experimental methods and Monte Carlo validation with a monoenergetic x-ray beam Med. Phys 45(4) 1724–1737 [PubMed: 29405311]

Fedon C, Caballo M and Sechopoulos I 2018b Internal breast dosimetry in mammography: Monte Carlo validation in homogeneous and anthropomorphic breast phantoms with a cinical mammograohy system accepted in Med. Phys

Friedewald SM et al. 2014 Breast cancer screening using tomosynthesis in combination with digital mammography JAMA 311(24) 2499–2507 [PubMed: 25058084]

García E, Diez Y, Diaz O, Lladó X, Gubern-Mérida A, Martí R, Martí J, and Oliver A 2018 Multimodal breast parenchymal patterns correlation using a patient-specific biomechanical model. IEEE Trans. on Medical Imaging 37(3) 712–723 [PubMed: 28885152]

Hammerstein GR, Miller DW, White DR, Masterson ME, Woodard HQ and Laughlin JS 1979 Absorbed radiation dose in mammography Radiology 130 485–491 [PubMed: 760167]

Hernandez AM, Seibert JA and Boone JM 2015 Breast dose in mammography is about 30% lower when realistic heterogeneous glandular distribution are considered Med. Phys 42 6337–6348 [PubMed: 26520725]

Hernandez AM and Boone JM 2014 Tungsten anode spectral model using interpolating cubic splines: unfiltered x-ray spectra from 20 kV to 640 kV Med. Phys 41 042101 [PubMed: 24694149]

Houssami N and Skaane P 2013 Overview of the evidence on digital breast tomosynthesis in breast cancer detection Breast 22(2) 101–108 [PubMed: 23422255]

Hsu CML, Palmeri ML, Segars WP, Veress A, Dobbins JT III 2011 An analysis of the mechanical parameters used for finite element compression of a high resolution 3D breast phantom Medical Physics 38 5756–5770 [PubMed: 21992390]

Huang SY, Boone JM, Yang K, Kwan ALC and Packard NJ 2008 The effect of skin thickness determined using breast CT on mammographic dosimetry Med. Phys 35(4) 1199–1206 [PubMed: 18491511]

Johnsen S and et al. 2014 NiftySim: A GPU-based nonlinear _finite element package for simulation of soft tissue biomechanics J. Comp. Assisted Radiology and Surgery 10(7) 1077–1095

Lagae A and Dutre P 2008 Compact, fast and robust grids for ray tracing Computer Graphics forum 27 (4) 1235–1244

Lång K, Andersson I, Rosso A, Tingberg A, Tingberg P and Zackrisson S 2016 Performance of one-view breast tomosynthesis as a stand-alone breast cancer screening modality: results from the Malmö Breast Tomosynthesis Screening Trial, a population-based study European Radiology 26(1) 184–190 [PubMed: 25929946]

Massera RT and Tomal A 2018 Skin models and their impact on mean glandular dose in mammography Phys. Med 18 S1120

Michell MJ and et al. 2012 A comparison of the accuracy of film-screen mammography, full-field digital mammography, and digital breast tomosynthesis Clin Radiol. 67 976–981 [PubMed: 22625656]

Miller K, Joldes G, Lance D, and Wittek A 2007 Total lagrangian explicit dynamics finite element algorithm for computing soft tissue deformation Comm. Num. Meth. Eng 23(2) 121–134

Ning R, Conover D, Yu Y, Zhang Y, Cai W, Betancourt-Benitez R and Lu X 2007 A novel cone beam breast CT scanner: System evaluation Proc. SPIE 6510 651030

Palomar AP, Calvo B, Herrero J, Lopez J and Doblare M 2008 A finite element model to accurately predict real deformations of the breast Medical Engineering and Physics 30 1089–1097 [PubMed: 18329940]

Pöhlmann STL, Lim YY, Harkness E, Pritchard S, Taylor CJ and Astley SM 2017 Three-dimensional segmentation of breast masses from digital breast tomosynthesis images JMI 4(3) 034007 [PubMed: 28948195]

Rafferty EA and et al. 2013 Assessing radiologist performance using combined digital mammography and breast tomosynthesis compared with digital mammography alone: results of a multicenter, multireader trial Radiology 267 47–56 [PubMed: 23297332]

Sechopoulos I, Suryanarayanan S, Vedantham S, D'Orsi CJ and Karellas A 2007 Computation of the glandular radiation dose in digital tomosynthesis of the breast Med. Phys 34(8) 221–232 [PubMed: 17278508]

Sechopoulos I, Feng SSJ and D'Orsi CJ 2010 Dosimetric characterization of a dedicated breast computed tomography clinical prototype Med. Phys 40 4110–4120

Sechopoulos I, Bliznakova K, Qin X, Fei B and Feng SSJ 2012 Characterization of the homogeneous tissue mixture approximation in breast imaging dosimetry Med. Phys 39(8) 5050–5059 [PubMed: 22894430]

Sechopoulos I 2013a A review of breast tomosynthesis. Part I. The image acquisition process Med. Phys 40 014301–014312 [PubMed: 23298126]

Sechopoulos I 2013b A review of breast tomosynthesis. Part II. The image reconstruction, processing and analysis, and advanced applications Med. Phys 40 014302–014317 [PubMed: 23298127]

Sempau J, Sánchez-Reyes A, Salvat F, Tahar HOB, Jiang SB and Fernández-Varea JM 2001 Monte Carlo simulation of electron beams from an accelerator head using PENELOPE Phys. Med. Biol 46 1163–1186 [PubMed: 11324958]

Skaane P and et al. 2012 Digital breast tomosynthesis (DBT): initial experience in a clinical setting Acta Radiol 53 524–529 [PubMed: 22593120]

Skaane P and et al. 2013 Comparison of digital Mammography Alone and Digital Mammography plus tomosynthesis in a population-based screening program Radiology 47–56

Stian FJ and et al. 2014 NiftySim: A GPU-based nonlinear finite element package for simulation of soft tissue biomechanics Int. J. CARS 10 1077–1095

Yaffe MJ, Boone JM, Packard N, Alonzo-Proulx O, Huang S-Y, Peresotti CL, Al-Mayah A and Brock K 2009 Themythof the 50–50 breast Med. Phys 36 5437–5443 [PubMed: 20095256]

Wellman P 1999 Tactile imaging *PhD thesis*, Cambridge, MA: Harvard University's Division of Engineering and Applied Sciences

Wu X, Barnes GT and Tucker DM 1991 Spectral dependence of glandular tissue dose in screen-film mammography. Radiology 179 143–148 [PubMed: 2006265]

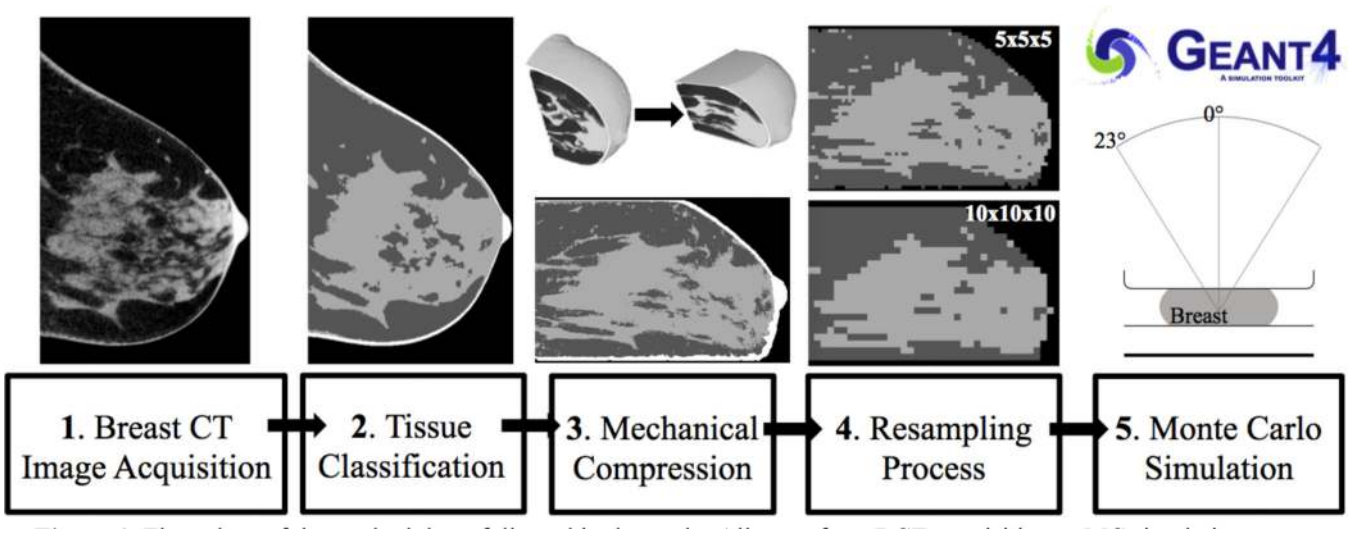

Figure 1:
Flow chart of the methodology followed in the study. All steps from BCT acquisition to MC simulation results are highlighted. Images are not to scale.

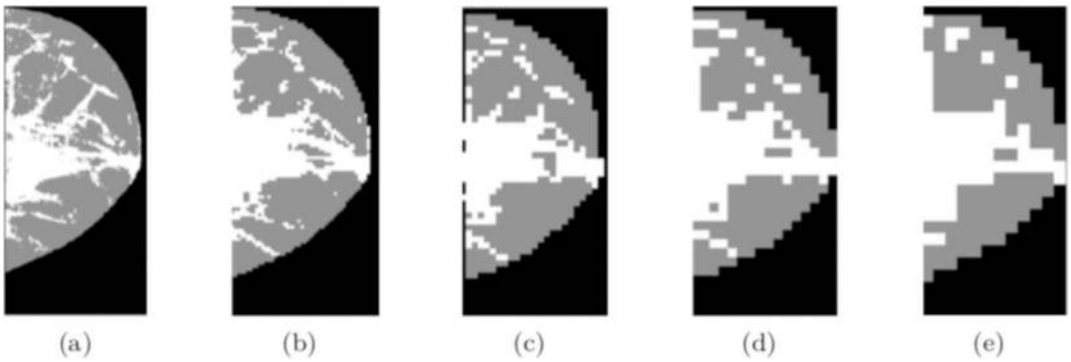

Figure 2:
Re-binning process on the XY axial plane. The same example slice is shown under the several anisotropic re-binning scenarios: (a) original voxel size, (b) $5 \times 5 \times 10$, (c) $10 \times 10 \times 10$, (d) $15 \times 15 \times 10$ and (e) $20 \times 20 \times 10$.

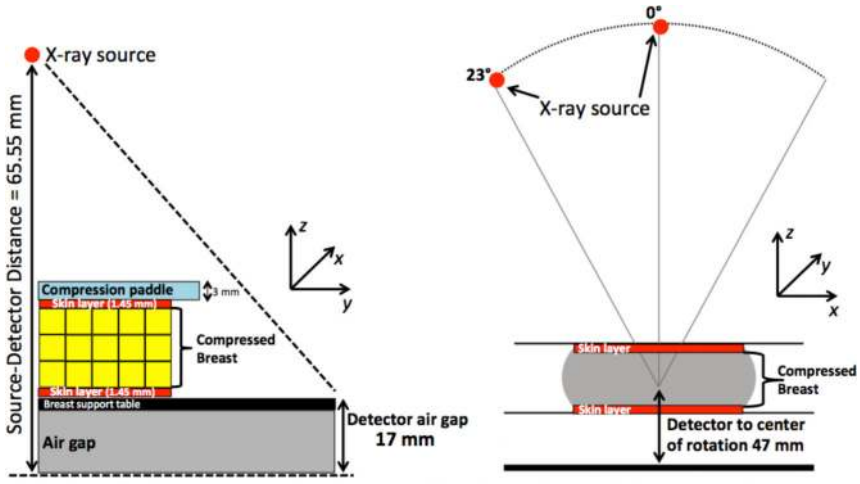

Figure 3:

Diagrams of the irradiation geometry implemented in the MC simulation. Drawings are not to scale.

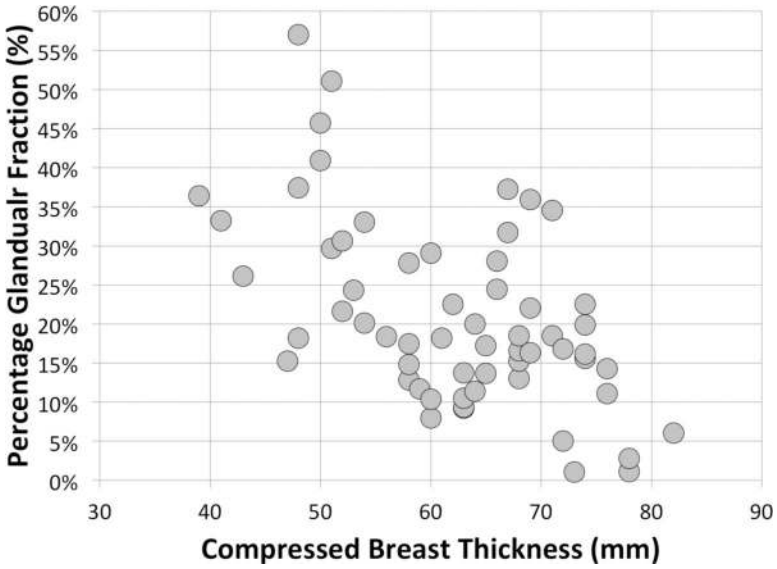

Figure 4:
Scatter plot of the patient study population (percentage glandular fraction versus compressed breast thickness).

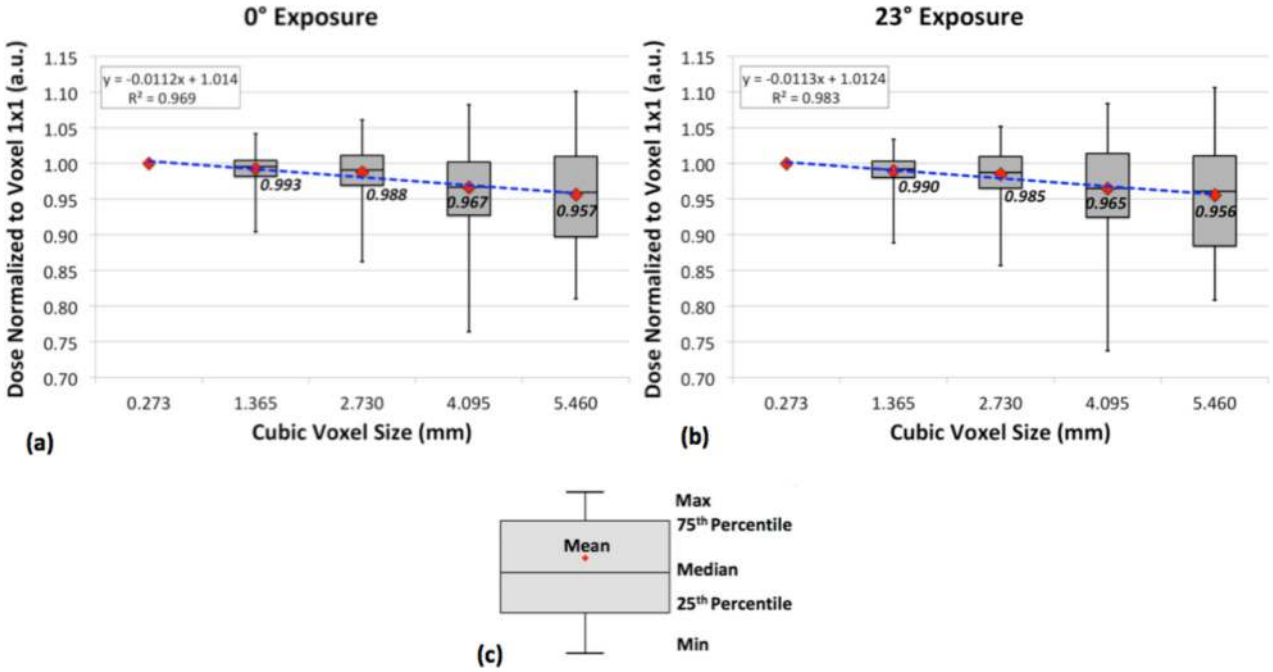

Figure 5:

Box-whisker plot of the normalized dose with respect to the reference level (voxel size 0.273 mm) for (a) 0° and (b) 23° exposure, respectively. The blue-dotted line corresponds to the linear fit. The specified numbers refers to the normalized mean dose values. (c) Box-whisker legend.

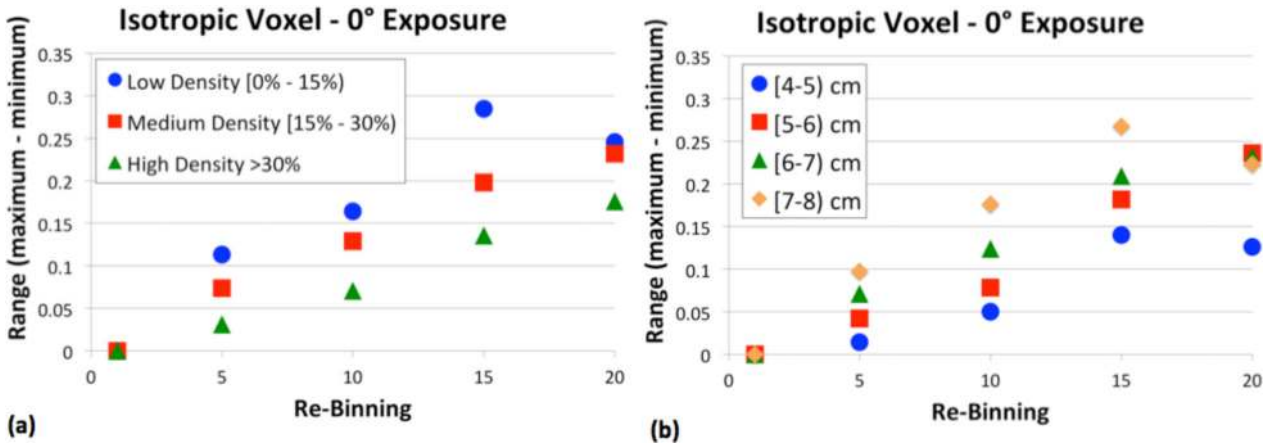

Figure 6:

Normalized dose range as a function of the isotropic re-binning case for 0° exposure (a) for different breast density and (b) for different compressed breast thickness.

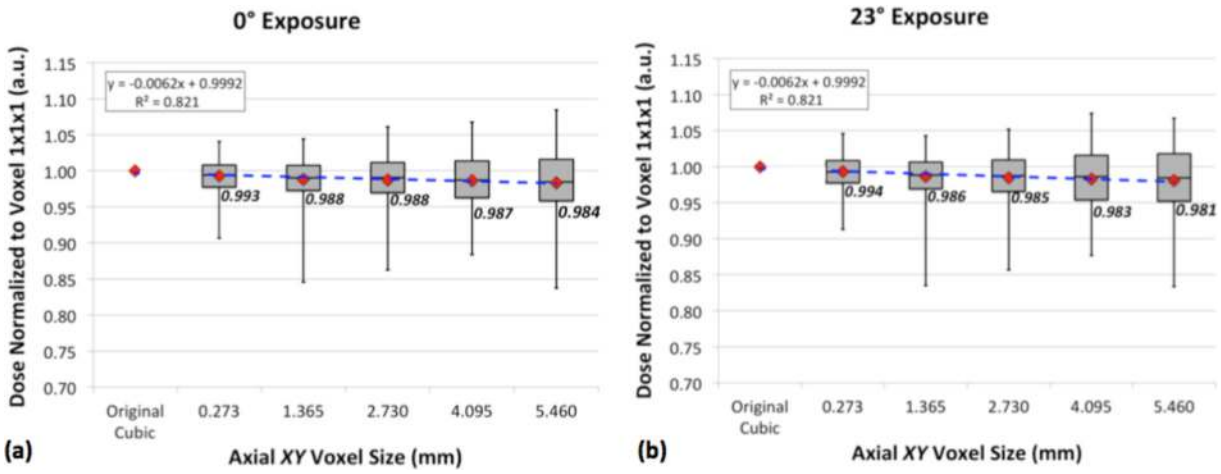

Figure 7:

Box-whisker plot of the normalized dose for a range of axial *XY* voxel sizes (*Z*-axis voxel size is fixed to 2.730 mm) for (a) 0° and (b) 23° exposure, respectively. The blue-dotted line corresponds to the linear fit. The specified numbers refers to the normalized mean dose values. Box-whisker legend is reported in Figure 5c.

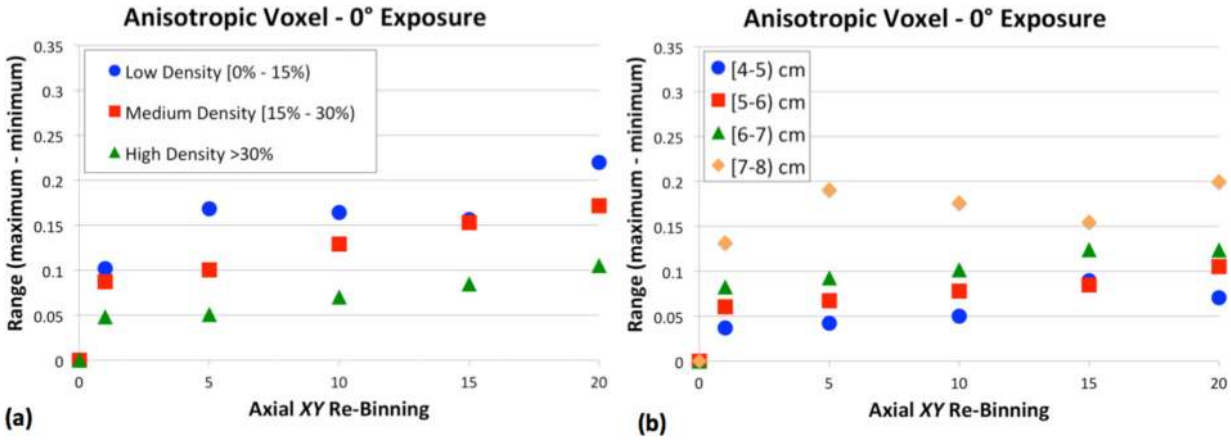

Figure 8:

Normalized dose range as a function of the anisotropic re-binning cases for 0° exposure (a) for different breast density and (b) for different compressed breast thickness.

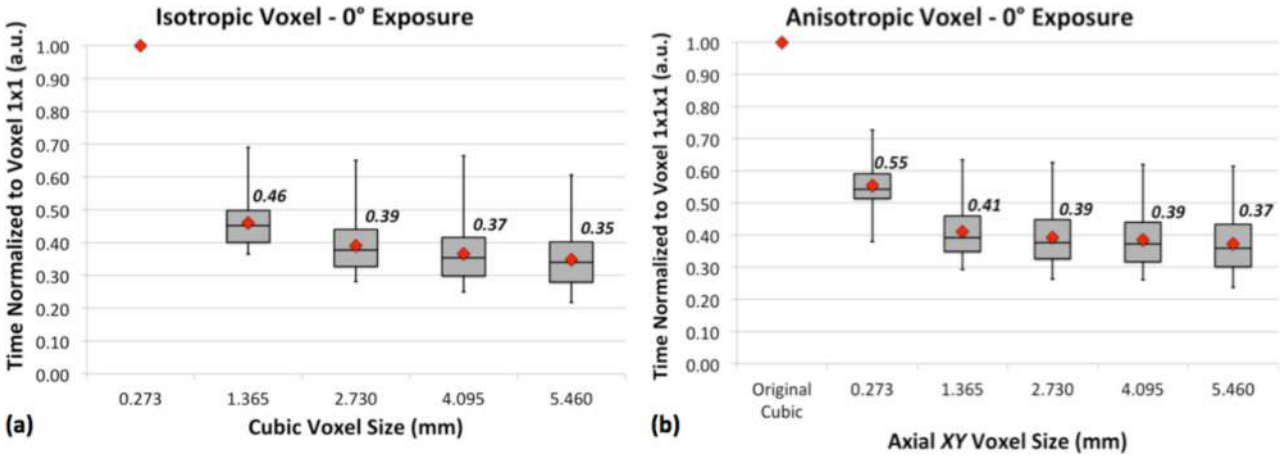

Figure 9:

Box-whisker plot showing the normalized simulation CPU time for (a) the different isotropic cubic voxel sizes and (b) anisotropic voxel investigated. The specified numbers refers to the normalized mean time values.

Table 1.

Scenarios investigated with the two re-binning approaches.

isotropic-voxel binning		anisotropic-voxel binning	
Binning	***Voxel Dimension (mm^3) (x, y, z)***	***Binning***	***Voxel Dimension (mm^3) (x, y, z)***
1 × 1 × 1	0.273 × 0.273 × 0.273	1 × 1 × 10	0.273 × 0.273 × 2.730
5 × 5 × 5	1.365 × 1.365 × 1.365	5 × 5 × 10	1.365 × 1.365 × 2.730
10 × 10 × 10	2.730 × 2.730 × 2.730	10 × 10 × 10	2.730 × 2.730 × 2.730
15 × 15 × 15	4.095 × 4.095 × 4.095	15 × 15 × 10	4.095 × 4.095 × 2.730
20 × 20 × 20	5.460 × 5.460 × 5.460	20 × 20 × 10	5.460 × 5.460 × 2.730

Table 2.

Target/filter, tube voltage and corresponding half value layer (in mm of Al) used in the Monte Carlo simulations as a function of the compressed breast thickness.

Compressed Breast Thickness (mm)	Target / Filter	Tube Voltage (kV)	1st Half Value Layer (mm Al)
30 – 39	W/ Rh	27	0.446
40 – 49	W/ Rh	28	0.455
50 – 59	W/ Rh	29	0.464
60 – 69	W/ Rh	30	0.471
70 – 79	W/ Rh	31	0.479
80 – 89	W/ Rh	32	0.486